4-8-2020

Hierarchical Plasmon Resonances in Fractal Structures

Isobel C. Bicket
McMaster University, bicketic@mcmaster.ca

Edson P. Bellido
McMaster University, bellidep@mcmaster.ca

Danielle M. McRae
The University of Western Ontario

Francois Lagugne-Labarthet
University of Western Ontario, flagugne@uwo.ca

Gianluigi A. Botton
McMaster University, gbotton@mcmaster.ca

Citation of this paper:
Isobel C. Bicket, Edson P. Bellido, Danielle M. McRae, François Lagugné-Labarthet, and Gianluigi A. Botton
ACS Photonics 2020 *7*(5), 1246-1254
DOI: 10.1021/acsphotonics.0c00110

Hierarchical Plasmon Resonances in Fractal Structures

Isobel C. Bicket,[*,†] Edson P. Bellido,[†] Danielle M. McRae,[‡] François Lagugné-Labarthet,[*,‡] and Gianluigi A. Botton[*,†,¶]

†*McMaster University, 1280 Main Street West, Hamilton, ON, Canada, L8S 4L8*

‡*The University of Western Ontario, 1151 Richmond Street, London, ON, Canada, N6A 5B7*

¶*Canadian Light Source, 44 Innovation Boulevard, Saskatoon, SK, Canada, S7N 2V3*

E-mail: bicketic@mcmaster.ca; flagugne@uwo.ca; gbotton@mcmaster.ca

Abstract

An equilateral triangular prism is used as the fundamental building block to construct additive Sierpiński fractals, enabling new surface plasmon resonances (SPR) in the first three generations of Sierpiński triangles, as well as topological intermediaries between generations. The modes are characterized using electron energy loss spectroscopy accompanied by eigenmode calculations and optical finite-difference time domain simulations. The complex fractal geometries present a predictable hierarchy of new resonances, each arising from the previous generational building blocks used to construct the fractal. Intermediate structures break the polarization degeneracy of the equilateral fractals while maintaining a rich multiband spectral response. Engineering defects in the narrow conductive channels of the fractal allows further manipulation of the SPR response, emphasizing higher order SPR modes over the lowest energy peak. The knowledge gained is used to develop guidelines for engineering the response

of more complex fractal-based structures, including the spectral response and hotspot distribution.

Keywords

Surface plasmon resonance, Sierpiński fractal, electron energy loss spectroscopy, hybridization, plasmonics, multiband antennas, self-similarity.

Metallic nanoprisms are structures of interest for numerous applications including sensing,[1,2] antennas,[3,4] non-linear optical processes[5,6] or optical rectification,[7] utilizing plasmonic properties that span a large spectral range. In these structures, the confinement of the electromagnetic field in sub-nanometer scale volumes can be further tuned by organizing them in geometries where the gaps between adjacent prisms further funnel photon energy into even smaller domains, with a drastic increase of the local fields. Prisms organized in pairs,[8,9] trimers,[10,11] pentamers[12] or more complex arrangements[13] have been shown to be of interest for enhanced optical processes due to the fine tuning of inter-prism gaps using electron beam lithography (EBL).

The Sierpiński fractal structure,[14] first studied for its multiband log-periodic resonances in GHz antennas,[15–19] presents an extension of the nanoprism geometry with a small spatial footprint and enhanced field confinement when used in bowtie antennas.[20–23] Due to the three-fold (C3) rotational symmetry of the Sierpinski fractal generations, these nanostructures are also of interest for second-order non-linear optical phenomena because of the absence of an inversion centre. The field confinement together with surface functionalization of a single nanoprism have been reported to yield second harmonic generation that can be exploited for photonic applications.[11,24]

To measure the energy and the spatial distribution of the plasmon modes in the vicinity of these structures, electron energy loss spectroscopy (EELS) associated with scanning transmission electron microscopy (STEM) is the technique of choice in terms of spatial resolution and sensitivity for both chemically synthesized[25] and lithographically fabricated nanostructures.[8,10,26,27] Furthermore, STEM-EELS reveals both the bright and dark modes, which, in conjunction with electromagnetic modelling, provide a comprehensive optical characterization of these structures.[28–32] STEM-EELS has been used to great effect in unravelling the complex hierarchy of plasmon resonance modes in fractal structures.[33]

In a previous work,[34] we used STEM-EELS to characterize silver nanoprisms organized in subtractive Sierpiński structures. Both positive and negative structures were fabricated by EBL. Using this approach, the energy and intensity of the plasmon resonance modes were measured for different fractal generations and for increasing cavity sizes. Key findings of this former work were (i) degenerate dipolar bright modes within the prisms couple with dipolar modes of the apertures, qualitatively obeying the Babinet principle; (ii) dipolar plasmon modes experience spectral redshifts when increasing the fractal generation or aperture size and reducing the width of conductive channels between building blocks; (iii) the overlap of the aperture with surface charge nodes of the plasmon modes causes spectral shifts, while overlap with resonance anti-nodes causes changes to the field distribution. However, the subtractive approach for fractal construction is inherently restricted by the spatial resolution of EBL, thus limiting the ability to inscribe higher generations with controlled sharpness and the understanding of energy shift and spatial distribution of the plasmon modes.

Herein, in order to lift these limitations, we investigate Sierpiński additive fractals, also referred to as diverging fractals. In this approach, prisms of the same dimensions are added sequentially to form the fractal structure. This arrangement of nanoprisms yields new plasmon resonances which can be explained by energy hybridization from previous fractal generations, as demonstrated by Bellido et al. on the Koch snowflake.[33] We report on how the advancement of the fractal generation, including partial generations, alters the optical properties of

the structure. In particular, using STEM-EELS together with calculation of the charge distributions and plasmon eigenmodes, we investigate the hybridization of dipolar modes from the zeroth to the third generation, enabling the prediction of the behaviour of subsequent generations with respect to the parent unit. Importantly, we show that new optical modes observed in the newer fractal generations can recursively be predicted from the previous generation: the self-similar hierarchy of the plasmon resonances follows the self-similarity of the fractal geometry. This work enables the prediction and manipulation of both the spatial and spectral positions of plasmon resonances in these hierarchical metastructures, properties that are necessary for molecular plasmonics applications in plasmon-enhanced spectroscopy, plasmon-mediated chemistry, or as passive photonic filters designed for specific spectral domains. This work also provides a general approach that can be extended to other types of hierarchical structures.

Results and Discussion

A constructive fractal is created starting from a single basic parent unit, referred to as generation 0 ('G0'). In the case of the Sierpiński fractal, the G0 unit is an equilateral triangular prism. Further fractal generations are built by using multiple copies of this fundamental structure. We construct a generation 1 ('G1') fractal from three G0 parents and a generation 2 ('G2') fractal from nine G0 grandparents, or three G1 parent units. We also construct topological intermediaries, which break the C3 symmetry, between fractal generations: G0.5 and G1.5, as shown in Figure 1.

We fabricate and characterize the fractal structures shown in Figure 2 using electron beam lithography and electron energy loss spectroscopy, respectively.[1,26,27] The spectral response of each structure becomes more and more complex as the fractal generation advances; each descendant generation will be discussed in turn, using eigenmode calculations (Figure 3) to reveal the origins of the increased spectral complexity, as demonstrated by Bellido et al.[33]

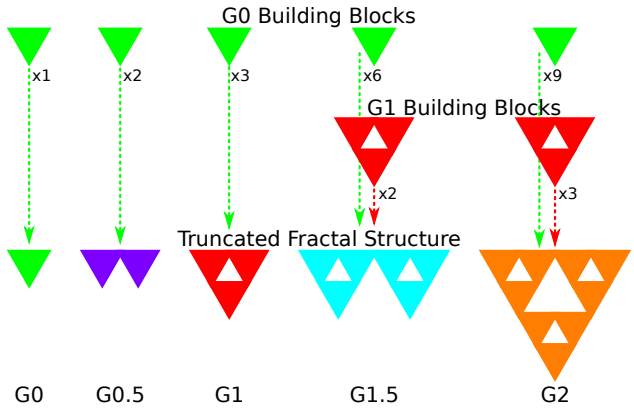

Figure 1: Truncated Sierpiński fractal generations are constructed from previous generations, starting with the fundamental equilateral triangle, using 3^n fundamental building blocks for the nth generation.

The origins of each of the eigenmodes depicted are assigned based on the number of nodes present in each sub-unit of the fractal structure. We study the hybridization of the G0 surface plasmon resonance dipolar modes in generations 0 through 2, including the intermediaries shown in Figure 1. Each successive fractal generation is larger than the previous generation and adds an additional response band through hybridization of the plasmon modes of the parent generations.

Generation 0

The G0 nanoprism, of side length 578 nm, exhibits the well-known set of SPR modes:[32,34,35] a degenerate pair of dipolar modes at the lowest energy (Figure 2(a, b)(i): peak 1 (0.52 eV)), followed by higher order edge modes (peaks 2 (0.94 eV), 3 (1.15 eV)) and finally cavity modes (peak 4 (1.67 eV), 5 (1.98 eV)). The EELS maps for the edge and cavity modes for all generations are presented in the Supplementary Information (Figure S1). The G0 nanoprism is the most basic structural building block and its dipolar modes form the basis for the plasmon resonances of descendant generations.

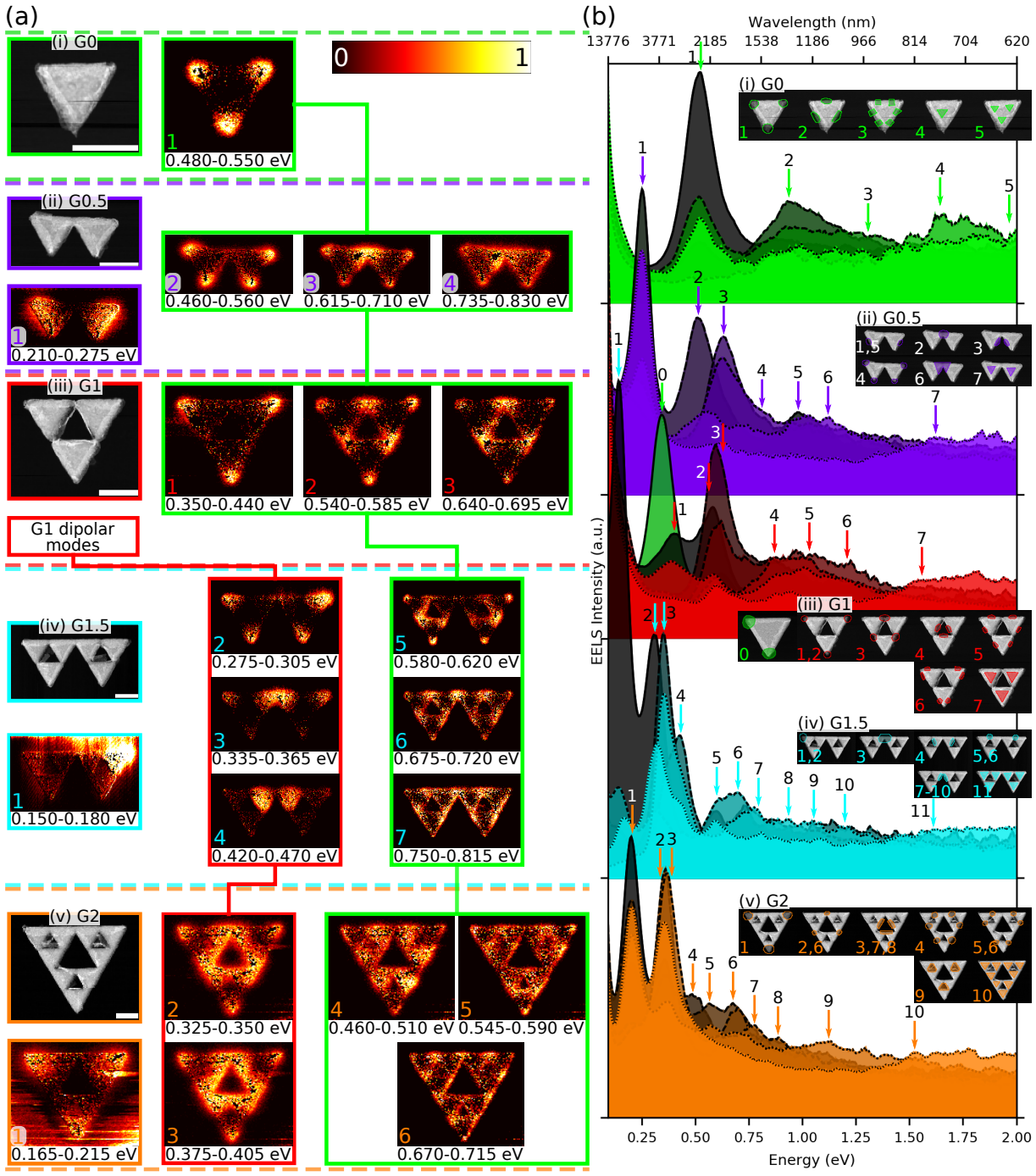

Figure 2: Experimental EELS data for G0, G0.5, G1, G1.5, and G2 structures. (a) HAADF images and EELS maps averaged over the energies indicated for the labelled peaks; all scalebars on HAADF images are 500 nm; connecting lines follow the hybridized descendant modes of the top mode through successive fractal generations; all EELS maps are individually normalized with EELS intensity mapped according to the colour scale in the upper right. A placeholder box is used instead of the G1 dipolar mode maps, which are not found in this structure because of the impaired conductive coupling. (b) EELS spectra for each of the structures in (a); insets indicate the areas from which each spectrum was extracted in the EELS spectrum image; each spectrum is normalized to the height of the zero loss peak.

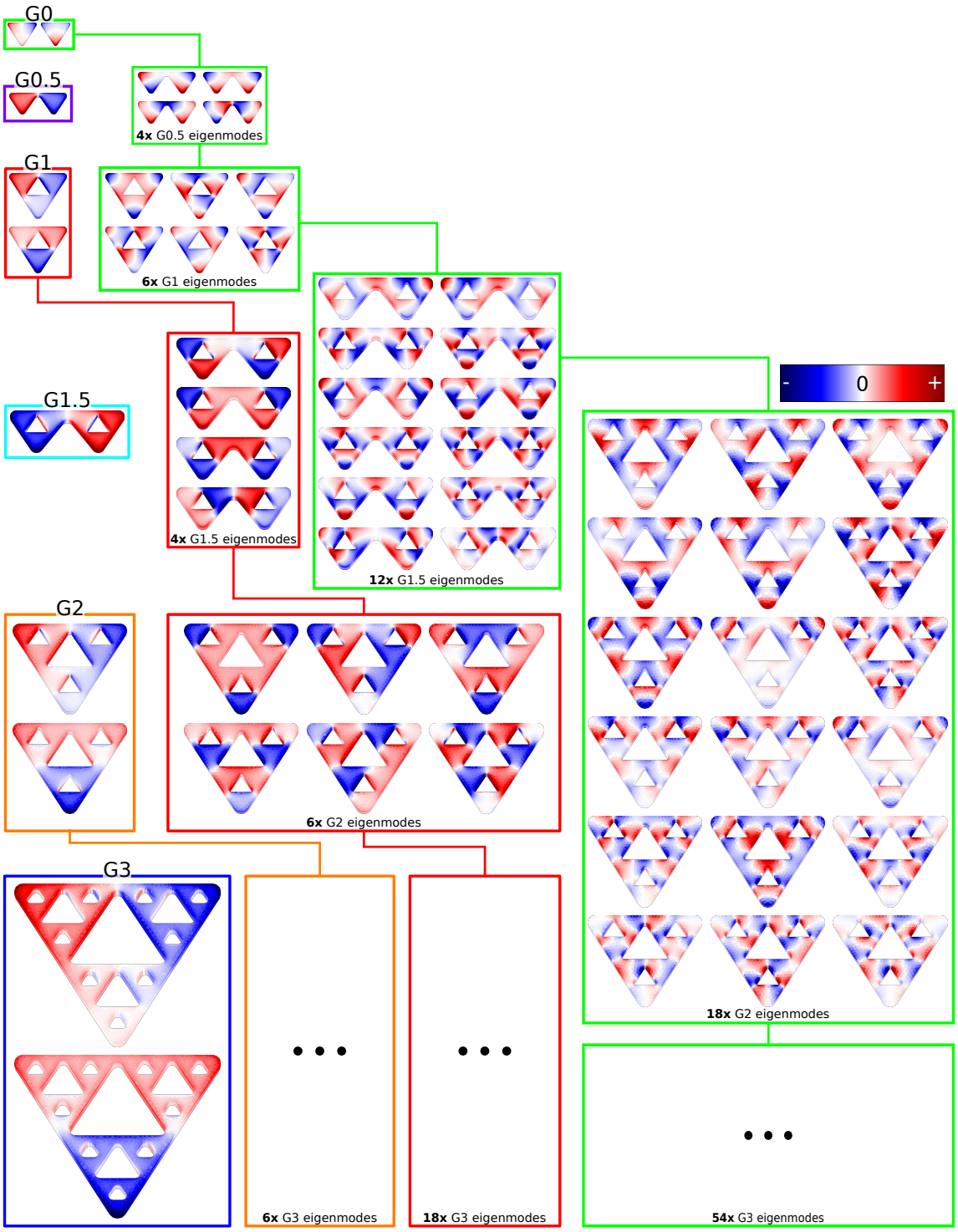

Figure 3: Eigenmode calculations of the hybridization of dipole modes of parent units as the fractal order is increased from G0 to G3. Connections show the hybridization dependence of dipole modes from previous generations, as determined by the number of surface charge nodes within each parent unit. Each element of the figure shows the surface charge distribution for each respective eigenmode; the colour scale for each eigenmode is normalized individually.

Generation 0.5

Using two G0 prisms to build an intermediate topology, we obtain the G0.5 structure. With one side twice as long as the G0 building block, the G0.5 structure possesses a strong peak at lower energy (Figure 2(b)(ii): peak 1 (0.25 eV)) than the G0 dipole peak (Figure 2(b)(i): peak 1 (0.52 eV)), followed by a cluster of three peaks close to each other in energy ((ii): peaks 2 (0.51 eV), 3 (0.63 eV), 4 (0.82 eV), and higher order edge modes ((ii): peaks 5 (0.98 eV), 6 (1.12 eV)).

The importance of conductive coupling between components in fractal structures has been emphasized in our previous work.[34] Conductive coupling between the prisms in this G0.5 structure is maintained, allowing a new dipolar mode across the whole structure to be sustained at low energy (Figure 2(a)(ii)): peak 1). Since the C3 symmetry present in the original equilateral triangle has been broken, there is only a single dipole mode in G0.5: the degeneracy and polarization-independence of the dipolar modes of the G0 parent have been broken. The two degenerate dipoles of the G0 parent hybridize to form four new eigenmodes in the G0.5 structure (Figure 3). From these four eigenmodes, three peaks are visible in the EELS data, identified by high EELS intensity around the corners of the G0 parents (Figure 2(a, b)(ii): peaks 2, 3, 4). The response from the G0 dipolar modes has split into a broader band in the new structure.

At higher energy than these modes, there are broader peaks from edge modes on the triangular G0 parents (Figure 2(b)(ii): peaks 5, 6). There is also a cavity mode at comparable energy to the G0 cavity mode (peak 7 (1.61 eV)). The cavity modes of each of the G0 parent units within the G0.5 structure are expected to hybridize to same-charge and opposite-charge cavity modes (similarly to higher order cavity modes seen in our previous work[34]). However, these are indistinguishable in conventional EELS data because it is not possible to differentiate symmetric and anti-symmetric cavity modes with different phases without resorting to beam-shaping techniques.[36] Small energy splitting between hybridized cavity modes, combined with more hybridizations of higher order cavity modes from each G0 parent

result in severe modal overlap and the appearance of a broad continuum of EELS signal above 1.5 eV (Figure 2(b)(ii): peak 7).

Generation 1

Completing the G1 structure by adding another G0 parent prism to the G0.5 nanostructure creates another set of hybridized modes. There are two new degenerate dipole modes in the G1 triangle (Figure 3) at a lower energy than the dipole modes of a similarly sized G0 structure[22,34] and six new modes from hybridizations of the G0 parent dipolar modes (Figure 3). In the experimentally fabricated G1 fractal presented in Figure 2(a, b)(iii), perfect conductive coupling across the structure is not maintained, and instead of new, lower energy dipolar modes, we see a set of three closely spaced peaks between 0.38 eV and 0.65 eV. The impaired conduction causes, instead of the expected redshift, a blueshift of the lowest energy mode.[8,10,22,34,37,38] These peaks are hybridized modes from coupled dipoles on each of the G0 parents,[34] as evidenced by the blueshift of the primary G1 peak compared to that of an equivalently-sized G0 prism (Figure 2(b)(iii): peak 0 (0.34 eV)).

With impaired conductivity across the whole G1 structure, the dipolar G0 modes split in energy to form peaks 1, 2, and 3 in Figure 2(b)(iii). Notably, the combination of the second and third peaks has a stronger EELS signal than the first, with high intensity at the tips of the G0 parents in the centre of each G1 edge (Figure 2(a)(iii): peaks 2, 3), indicating that it may be possible to use the conductivity between fractal parent units to control the relative strengths of different spectral response bands. We also detect higher order edge modes (peaks 4, 5, 6 (between 0.84 and 1.25 eV)) and the first cavity mode (peak 7 (1.52 eV)) in this G1 fractal. Similarly to the G0.5 case, we expect multiple cavity mode configurations from hybridization on the three parent units and we do not see a single distinct cavity mode peak, but only the onset of signal on the faces of the G0 parents within the G1 fractal, beginning at approximately the energy of the primary G0 cavity mode.

Generation 1.5

In the G1.5 structure, built from two G1 parent units or six G0 grandparent units (Figure 1), and shown in Figure 2(a, b)(iv), there is conductive coupling across the whole structure. A single dipole mode is present at 0.165 eV (Figure 2(a, b)(iv): peak 1); similarly to the G0.5 intermediate structure, the C3 symmetry of the standard Sierpiński fractal is broken and the dipolar mode is polarization-selective along the long axis of the G1.5 structure (Figure 3). In the experimental data, the energy of the G1.5 dipolar mode is approaching the limits of the instrument resolution, and some artefacts are visible in the peak map (Figure 2(a)(iv): peak 1). Within this map, small high frequency modulations are visible, caused by fluctuations in the shape of the zero loss peak of the microscope due to ripple in the high tension supply tank. There is also high intensity towards the top of the image caused by distortions to the spectrum from the flyback of the electron beam as it rasters over the sample. Despite these artefacts at the edge of the frame, the presence of the EELS peak is significantly correlated with the outer corners of the G1.5 structure.

At higher energy, there are three peaks in the EELS data between 0.3 and 0.42 eV (peaks 2-4) and four eigenmodes (Figure 3) arising from hybridization of the two degenerate dipole modes of the G1 parent fractal and broadening the spectral response in this energy range compared to the G1 parent. Dipolar modes from the G0 grandparent hybridize in the G1.5 structure to form 12 new eigenmodes (Figure 3). Experimentally, these eigenmodes are very close to each other in energy and spatial distribution; they form a spectral band slightly blueshifted from the G0 dipolar response, in the form of a series of peaks between 0.5 and 0.82 eV (Figure 2(a, b)(iv): peaks 5-7) with high intensity at the tips of the G0 grandparents, resembling peaks 2-4 of the G0.5 structure. The next spectral band in the EELS data, from 0.84 to 1.30 eV, contains edge modes from hybridization of the higher order G0 grandparent edge modes (peaks 8-10), followed by a broad signal starting at 1.55 eV (peak 11) from hybridization of G0 cavity modes. Cavity mode hybridization is very complex in higher order fractals, as there are now six G0 parents, and the modes are truly blurred out and

indistinguishable from the EELS data.

Generation 2

By stepping from G1.5 to G2, the three-fold symmetry is restored and there are again two new degenerate dipole modes across the whole prism (Figure 2(b)(v): peak 1 (0.19 eV); and Figure 3). Adding the third G1 triangle to the fractal blueshifts the dipolar mode of G2 relative to G1.5 and restores the polarization insensitivity. The low energy of the dipolar peak and the large size of the G2 structure (now 2290 nm along each side) result in some instrumental artefacts appearing in the lower corners of the peak map (Figure 2(a)(v): peak 1) from misalignment in the descan system of the microscope. Clear evidence of the presence of the dipolar mode remains in the high EELS intensity at the corners of the G2 prism. Optical simulations confirm that the G2 possesses two orthogonal, degenerate dipolar responses when conductive coupling is maintained across the whole structure (Figure 4(a),(b)(v): peak 1). Electric field responses for each of the peaks presented in Figure 4(a) can be found in the Supplementary Information.

The dipole modes of the G1 parent hybridize in the G2 structure to form six eigenmodes, from which only two peaks are resolvable in the EELS data acquired (Figure 2(b)(v): peak 2 (0.34 eV), 3 (0.39 eV)) and the optical simulations (Figure 4(a),(b)(v): peak 2, 3). As revealed by the optical simulations, each of these peaks is a pair of orthogonal degenerate modes. The second peak of this pair (peak 3) has the strongest scattering cross-section and, notably, is sharper then the similar peak on either G0 or G1 of the same size (Figure 4(b)(iii-v)) and stronger than the dipolar peak of the G1 parent (Figure 4(b)(ii)). The Sierpiński fractal structure, when used as a radio antenna, shows multiband optical responses;[16] the increasing definition of peak 3 in the optical spectra and in the EELS signal indicates that the response of higher order modes can rival that of the dipolar mode in fractal nanoantennas.

Dipolar modes from the G0 grandparent hybridize to form 18 eigenmodes (Figure 3) in the G2 structure. The high symmetry of the structure and the close energy spacing of all

of these modes means that most of these modes are indistinguishable experimentally; three peaks can be distinguished in the EELS data between 0.46 and 0.71 eV (Figure 2(b)(v): peaks 4, 5, 6), and we identify these as arising from hybridization of the G0 dipolar modes by the localization of EELS signal around the corners of the G0 grandparent units and the proximity in energy to the G0 grandparent dipolar peak. Optically, two pairs of degenerate modes arise from G0 dipolar mode hybridization (Figure 4(a),(b)(v): peaks 4, 5), though the SPR modes may be close enough in energy that the responses are mixing with each other and individual modes cannot be easily separated anymore. Although the first of these peaks (peak 4) is optically weak, the second is a clearly defined peak with a stronger scattering cross-section than the dipolar peak of the G0 grandparent (Figure 4(b)(i)).

At higher energy than these peaks is a broad amalgam of peaks identified as hybridizations of edge modes of the G0 prism (Figure 2(a, b)(v): peaks 7, 8; Figure 4(a),(b)(v): peaks 6-8) and aperture modes around the edges of the G2 apertures (Figure 2(a, b)(v): peak 9), which come from perturbed cavity modes of previous generation structures.[34] The final identifiable spectral response (peak 10) is identified as a descendant of the G0 primary cavity mode (Figure 2(a, b)(i): peak 4).

Predicting Recursive Modes

Using the experimental results supported by calculations, we can, in a manner extensible to other hierarchical structures, predict the recursive trend of SPR modes in increasing generational orders of fractals. There are two degenerate dipole modes on the G0 parent which hybridize to form $2(3^n)$ modes on an nth generation fractal with 3^n G0 parent units. Each successive fractal generation acts as a larger parent unit for the next generation, revealing similar SPR behaviour to the G0 hybridized modes, but on another length scale; in higher fractal generations, modes arising from hybridization of the G1 dipolar modes will number $2(3^{n-1})$. The trend is confirmed by examining the predicted eigenmodes of a Generation 3 (G3) ($n = 3$) fractal structure (Figure 3), which has $2(3^0) = 2$ degenerate dipole modes;

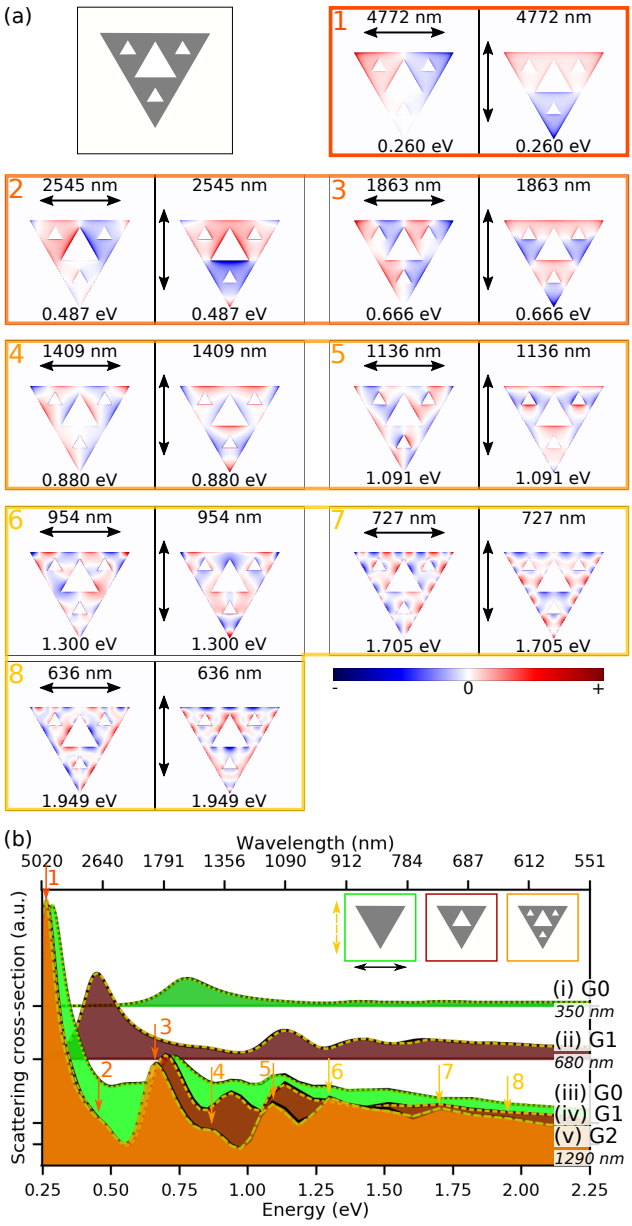

Figure 4: Optical FDTD simulations for three fractal generations. (a) Surface charge density distributions at the indicated wavelength, energy, and polarization, grouped by hybridization origin of plasmon modes, for a G2 fractal of side length 1290 nm; (b) spectra for (i) G0 fractal of side length 350 nm (green), (ii) G1 fractal of side length 680 nm (dark red), (iii, iv, v) G0 (green), G1 (dark red), and G2 (orange) fractals, respectively, of side length 1290 nm for vertical (yellow dashed lines) and horizontal (black solid lines) polarized light at normal incidence. Each individual distribution plotted in (a) is scaled individually according to the colour scale shown in the lower right.

$2(3^1) = 6$ dipole modes resulting from hybridization of the G2 parent unit dipolar modes; $2(3^2) = 18$ eigenmodes resulting from hybridization of the G1 grandparent unit dipolar modes; and $2(3^3) = 54$ eigenmodes resulting from hybridization of the G0 great-grandparent dipolar modes. Extrapolating from these results, we may predict that, for instance, a Generation 8 fractal will have two degenerate dipole modes, six modes resulting from hybridization of the G7 dipole modes, and so on, down to 13,122 eigenmodes arising from hybridization of the G0 dipolar modes. We also note that, because of the C3 symmetry of each full fractal generation, each pair of dipolar modes in the Sierpiński fractal actually represents a set of six degenerate dipole modes, which can be obtained by rotations of 120°.

Experimentally, many of these different hybridized modes will be degenerate or indistinguishable from each other after taking into account instrument resolution and intrinsic peak width, especially for the higher order modes present in the smaller parent units of each generation. Each successive fractal generation adds a new band to the response spectrum while maintaining and broadening the response from all of the previous generations. The localized hotspots for each mode can be predicted through knowledge of which band the mode is in: the hotspots for each mode, as visualized through EELS, tend to occur at locations relevant to the fractal parent units from which that band arises, as observed in the current example of the Sierpiński fractal and in other self-similar hierarchical geometries.[33,39–41]

The fractal nature of the structures contributes to some of the unique properties of the plasmon response spectrum. The symmetry of many deterministic fractals is consistent across all length scales;[42] the repetitive self-similar symmetry of geometrical fractals such as the Sierpiński is evident from inspection of different generations. Each successive generation maintains the C3 symmetry of the previous generations. The self-similarity of the geometrical symmetry is also reflected in the anisotropy of the plasmon response across the different spectral bands in each generation. Each of the plasmon modes in which the charge distribution breaks the C3 symmetry is partnered with a degenerate mode which responds to the opposite polarization (Figure 4), thereby maintaining the anisotropy of the response

regardless of generation number. We may also predict that in higher generations, the fractal geometry ensures that each plasmon resonance mode either has C3 symmetry or orthogonal degeneracy. Considering the G1 fractal, we notice that the charge distribution and EELS map of the hybridized modes from the G0 dipole maintain the same symmetry as higher order edge modes on the simple G0 nanoprism, but with stronger scattering cross-sections; these symmetries are repeated through all generations.

In addition, the repetition of the G0 parent unit is reflected in the strength of higher order plasmon modes. Compared to other hierarchical structures, such as a simple chain of coupled nanoparticles,[43,44] higher order modes in the Sierpiński fractal structure have a stronger response relative to the dipole peak with increasing generation number (Figure 2 (b), 4 (b)), confirming trends seen in Cesaro fractals,[39] Koch fractals,[33] and Cayley trees,[41] among others.[45]

The self-similar recursive trend described herein is possible only because of the conductive coupling between the parent prisms in each fractal generation, allowing charge to flow completely into or out of each parent unit. Breaking the conductive coupling within the Sierpiński fractal eliminates the low energy dipolar modes and leads to sets of three-way, or n-way hybridized modes based on coupling between the parent units, as seen in the G1 fractal presented in this work. The presence of defects in the structure which impair conductive coupling provides another way to manipulate the spectral response of the fractal structure. Introducing defects blueshifts the response and promotes the intensity of higher order peaks over the lowest energy peak.

The intermediate topologies (G0.5 and G1.5) present interesting cases in which the dipolar peak is strongly redshifted relative to succeeding fractal generations of the same size, and the dipolar degeneracy is broken, leading to a polarization-sensitive response. Despite the dipolar redshift and breaking of the C3 symmetry, these halfway structures still present a similar multiband response from hybridization of the modes of the parent generations; the intermediate structures present themselves as candidates for multiband, polarization-sensitive

sensing platforms.

Conclusions

We have shown how the basic elements of a fractal structure can be used to effectively design multiband spectral responses with predictable localized hotspots in hierarchical structures. Through fine-tuning of the fabrication parameters, we can introduce defects to further manipulate the spectral response; by reducing conduction between the parent units, we enhance the signal from higher order peaks and blueshift the energy of the lowest order set of peaks. The possibility of defect engineering combined with the polarization-sensitivity of the intermediate topologies with distinct symmetries provides interesting opportunities for multiband sensing platforms or second harmonic generation with rich polarization-dependent spectral responses by, for instance, leaving only one conductive channel in a G1 fractal.

Each previous generation within a fractal structure contributes a spectral response band through hybridization of its dipolar modes; the number of eigenmodes arising from each parent unit can be predicted by applying a simple equation. Similar modes are seen on different length scales within the fractal structure, exhibiting a hierarchical response which is strongly linked to the hierarchical geometry and use of fundamental building blocks. This makes the fractal structure a strong candidate for multiband sensing applications; more spectral bands with strong scattering probabilities can be added by increasing the number of iterations used to construct the fractal. The complex fractal structures constructed from basic building blocks show predictable responses, providing valuable tools for the manipulation of plasmon modes and engineering design strategies for tuning the multiband response.

Methods

Simulations

FDTD

The electromagnetic fields and surface charge distributions of the Sierpiński fractal metamaterials were simulated using the finite-difference time-domain (FDTD) method (Lumerical FDTD Solutions). The size of the fractal structure was as described in the text, using the dielectric function of silver from Palik.[46] The structures were 30 nm thick. The fractal structure was simulated on a substrate of SiN, modelled using the dielectric function from Luke.[47]

The maximum mesh size was set to at least 10 mesh cells per wavelength. The Sierpiński fractal structures were meshed by 6.5 nm in x and y, and 2 nm in z. The symmetry of the structure was exploited in order to reduce computation time, by application of a symmetry boundary condition along the minimum boundary in the x-direction. Perfectly matched layers (PML) were applied along all other boundaries, in order to truncate the simulation region.

BEM

The Metallic Nanoparticle Boundary Element Method (MNPBEM)[48] toolbox was used to calculate the eigenmodes of the Sierpiński fractal structures. The dielectric function for silver from Johnson and Christy[49] was used for all of the structures. G0 to G2 triangles for the hybridization study were 620 nm on each side and the G3 triangles were larger to accommodate the smaller apertures without errors in the meshing, with a side length of 1240 nm. Each triangle was 30 nm thick. Eigenmodes are calculated in the quasistatic approximation and the change in size only affects the energy of the mode, not the spatial distribution of charges.[50]

Sample Fabrication

Electron beam lithography was performed using a JEOL-JSM 7000F SEM equipped with Nanometer Pattern Generation System (NPGS). The structures were fabricated on TEM grids, each with nine separate 50 nm thick silicon nitride membrane windows. The e-beam resist used was 950 kg/mol poly(methyl methacrylate), 3% in anisole, which was spincoated onto the TEM grids at 6k RPM for 90 seconds. A post-bake was performed at 175°C for five minutes before pattern writing. Development of the exposed patterns was done for 2 minutes in methyl isobutyl ketone in isopropanol (MIBK:IPA), then 30 nm of silver was deposited using electron beam evaporation, before lift-off in acetone.

Electron Energy Loss Spectroscopy

A monochromated FEI Titan scanning transmission electron microscope, operated at 80 kV, with a Gatan Tridiem (model 865) spectrometer, was used to acquire electron energy loss spectroscopy (EELS) data. Post-processing treatment of the data was done using a custom Python software,[51] to first perform Richardson-Lucy deconvolution, and then to extract averaged spectra from selected areas or 2D EELS intensity maps across selected energy ranges. Each spectrum is normalized to the spectral integral before deconvolution. The deconvolution algorithm[52] serves to reduce the contribution of the zero loss peak (ZLP) to the signal from the sample, and improves the energy resolution from approximately 60 meV (full width at half maximum of the ZLP) in the raw data to approximately 40 meV. 15 iterations of the Richardson-Lucy algorithm were used on all of the EELS datasets, except for the G1.5 structure, for which 30 iterations were used to reveal the low energy dipole peak.

Acknowledgements

I.C.B, E.P.B, F.L.L., and G.A.B gratefully acknowledge support from the Natural Sciences and Engineering Research Council (NSERC) under the Discovery Grant program. Experimental EELS work was carried out at the Canadian Centre for Electron Microscopy (CCEM), a national facility supported by the Canada Foundation for Innovation under the Major Science Initiatives program, NSERC, and McMaster University.

Supporting Information Available

- HierarchicalFractalsSI.pdf: Supporting information and figures – edge and cavity mode EELS maps for all generations and FDTD calculations of the electric fields for the G2 structures.

This material is available free of charge via the Internet at http://pubs.acs.org.

References

(1) Duan, H.; Hu, H.; Kumar, K.; Shen, Z.; Yang, J. K. W. Direct and Reliable Patterning of Plasmonic Nanostructures with Sub-10-nm Gaps. *ACS Nano* **2011**, *5*, 7593–7600.

(2) Tabatabaei, M.; Wallace, G. Q.; Caetano, F. A.; Gillies, E. R.; Ferguson, S. S. G.; Lagugné-Labarthet, F. Controlled positioning of analytes and cells on a plasmonic platform for glycan sensing using surface enhanced Raman spectroscopy. *Chem. Sci.* **2016**, *7*, 575–582.

(3) Rang, M.; Jones, A. C.; Zhou, F.; Li, Z.-Y.; Wiley, B. J.; Xia, Y.; Raschke, M. B. Optical Near-Field Mapping of Plasmonic Nanoprisms. *Nano Lett.* **2008**, *8*, 3357–3363.

(4) Rosen, D. A.; Tao, A. R. Modeling the Optical Properties of Bowtie Antenna Generated By Self-Assembled Ag Triangular Nanoprisms. *ACS Appl. Mater. Interfaces* **2014**, *6*, 4134–4142.

(5) Li, Z.; Yu, Y.; Chen, Z.; Liu, T.; Zhou, Z.-K.; Han, J.-B.; Li, J.; Jin, C.; Wang, X. Ultrafast Third-Order Optical Nonlinearity in Au Triangular Nanoprism with Strong Dipole and Quadrupole Plasmon Resonance. *J. Phys. Chem. C* **2013**, *117*, 20127–20132.

(6) Salomon, A.; Zielinski, M.; Kolkowski, R.; Zyss, J.; Prior, Y. Size and Shape Resonances in Second Harmonic Generation from Silver Nanocavities. *J. Phys. Chem. C* **2013**, *117*, 22377–22382.

(7) Gadalla, M. N.; Abdel-Rahman, M.; Shamim, A. Design, Optimization and Fabrication of a 28.3 THz Nano-Rectenna for Infrared Detection and Rectification. *Sci. Rep.* **2014**, *4*, 1–9.

(8) Duan, H.; Fernández-Domínguez, A. I.; Bosman, M.; Maier, S. A.; Yang, J. K. W.

Nanoplasmonics: Classical down to the Nanometer Scale. *Nano Lett.* **2012**, *12*, 1683–1689.

(9) Garreau, A.; Tabatabaei, M.; Hou, R.; Wallace, G. Q.; Norton, P. R.; Lagugné-Labarthet, F. Probing the Plasmonic Properties of Heterometallic Nanoprisms with Near-Field Fluorescence Microscopy. *J. Phys. Chem. C* **2016**, *120*, 20267–20276.

(10) Koh, A. L.; Fernández-Domínguez, A. I.; McComb, D. W.; Maier, S. A.; Yang, J. K. W. High-Resolution Mapping of Electron-Beam-Excited Plasmon Modes in Lithographically Defined Gold Nanostructures. *Nano Lett.* **2011**, *11*, 1323–1330.

(11) Hou, R.; Shynkar, V.; Lafargue, C.; Kolkowski, R.; Zyss, J.; Lagugné-Labarthet, F. Second Harmonic Generation from Gold Meta-molecules with Three-fold Symmetry. *Phys. Chem. Chem. Phys.* **2016**, *18*, 7956–7965.

(12) Segal, E.; Galanty, M.; Aharon, H.; Salomon, A. Visualization of Plasmon-Induced Hot Electrons by Scanning Electron Microscopy. *J. Phys. Chem. C* **2019**, *123*, 30528–30535.

(13) Wallace, G. Q.; Tabatabaei, M.; Hou, R.; Coady, M. J.; Norton, P. R.; Simpson, T. S.; Rosendahl, S. M.; Merlen, A.; Lagugné-Labarthet, F. Superimposed Arrays of Nanoprisms for Multispectral Molecular Plasmonics. *ACS Photonics* **2016**, *3*, 1723–1732.

(14) Sierpinski, W. Sur une courbe dont tout point est un point de ramification. *C.R. Hebd. Acad. Sci.* **1915**, *160*, 302–305.

(15) Puente, C.; Romeu, J.; Pous, R.; Garcia, X.; Benitez, F. Fractal multiband antenna based on the Sierpinski gasket. *Electron. Lett.* **1996**, *32*, 1–2.

(16) Puente-Baliarda, C.; Romeu, J.; Pous, R.; Cardama, A. On the Behavior of the Sierpinski Multiband Fractal Antenna. *IEEE T. Antenn. Propag.* **1998**, *46*, 517–524.

(17) Borja, C.; Romeu, J. Multiband Sierpinski fractal patch antenna. IEEE Antennas and Propagation Society International Symposium. 2000; pp 1708–1711 vol.3.

(18) Baliarda, C. P.; Borau, C. B.; Rodero, M. N.; Robert, J. R. An iterative model for fractal antennas: application to the Sierpinski gasket antenna. *IEEE T. Antenn. Propag.* **2000**, *48*, 713–719.

(19) Romeu, J.; Soler, J. Generalized Sierpinski fractal multiband antenna. *IEEE T. Antenn. Propag.* **2001**, *49*, 1237–1239.

(20) Anguera, J.; Puente, C.; Borja, C.; Montero, R.; Soler, J. Small and High-Directivity Bow-tie Patch Antenna Based on the Sierpinski Fractal. *Microw. Opt. Techn. Let.* **2001**, *31*, 239–241.

(21) Sederberg, S.; Elezzabi, A. Y. Sierpiński Fractal Plasmonic Antenna: a Fractal Abstraction of the Plasmonic Bowtie Antenna. *Opt. Express* **2011**, *19*, 10456–10461.

(22) Cakmakyapan, S.; Cinel, N. A.; Cakmak, A. O.; Ozbay, E. Validation of Electromagnetic Field Enhancement in Near-Infrared through Sierpinski Fractal Nanoantennas. *Opt. Express* **2014**, *22*, 19504–19512.

(23) Seitl, L.; Laible, F.; Dickreuter, S.; Gollmer, D. A.; Kern, D. P.; Fleischer, M. Miniaturized Fractal Optical Nanoantennas Defined by Focused Helium Ion Beam Milling. *Nanotechnology* **2019**, *31*, 075301.

(24) Salomon, A.; Prior, Y.; Fedoruk, M.; Feldmann, J.; Kolkowski, R.; Zyss, J. Plasmonic Coupling between Metallic Nanocavities. *J. Opt.* **2014**, *16*, 114012.

(25) Nelayah, J.; Kociak, M.; Stéphan, O.; García de Abajo, F. J.; Tencé, M.; Henrard, L.; Taverna, D.; Pastoriza-Santos, I.; Liz-Marzán, L. M.; Colliex, C. Mapping surface plasmons on a single metallic nanoparticle. *Nat. Phys.* **2007**, *3*, 348–353.

(26) Boudarham, G.; Feth, N.; Myroshnychenko, V.; Linden, S.; García de Abajo, J.; Wegener, M.; Kociak, M. Spectral Imaging of Individual Split-Ring Resonators. *Phys. Rev. Lett.* **2010**, *105*.

(27) Koh, A. L.; McComb, D. W.; Maier, S. A.; Low, H. Y.; Yang, J. K. W. Sub-10 nm patterning of gold nanostructures on silicon-nitride membranes for plasmon mapping with electron energy-loss spectroscopy. *J. Vac. Sci. Technol. B* **2010**, *28*, C6O45–C6O49.

(28) Chu, M.-W.; Myroshnychenko, V.; Chen, C. H.; Deng, J.-P.; Mou, C.-Y.; García de Abajo, F. J. Probing Bright and Dark Surface-Plasmon Modes in Individual and Coupled Noble Metal Nanoparticles Using an Electron Beam. *Nano Lett.* **2009**, *9*, 399–404.

(29) Koh, A. L.; Bao, K.; Khan, I.; Smith, W. E.; Kothleitner, G.; Nordlander, P.; Maier, S. A.; McComb, D. W. Electron Energy-Loss Spectroscopy (EELS) of Surface Plasmons in Single Silver Nanoparticles and Dimers: Influence of Beam Damage and Mapping of Dark Modes. *ACS Nano* **2009**, *3*, 3015–3022.

(30) Schmidt, F.-P.; Ditlbacher, H.; Hohenester, U.; Hohenau, A.; Hofer, F.; Krenn, J. R. Dark Plasmonic Breathing Modes in Silver Nanodisks. *Nano Lett.* **2012**, *12*, 5780–5783.

(31) Bellido, E. P.; Manjavacas, A.; Zhang, Y.; Cao, Y.; Nordlander, P.; Botton, G. A. Electron Energy-Loss Spectroscopy of Multipolar Edge and Cavity Modes in Silver Nanosquares. *ACS Photonics* **2016**, *3*, 428–433.

(32) Keast, V. J.; Walhout, C. J.; Pedersen, T.; Shahcheraghi, N.; Cortie, M. B.; Mitchell, D. R. G. Higher Order Plasmonic Modes Excited in Ag Triangular Nanoplates by an Electron Beam. *Plasmonics* **2016**, *11*, 1081–1086.

(33) Bellido, E. P.; Bernasconi, G. D.; Rossouw, D.; Butet, J.; Martin, O. J. F.; Botton, G. A. Self-Similarity of Plasmon Edge Modes on Koch Fractal Antennas. *ACS Nano* **2017**, *11*, 11240–11249.

(34) Bicket, I. C.; Bellido, E. P.; McRae, D. M.; Lagugné-Labarthet, F.; Botton, G. A. Carving Plasmon Modes in Silver Sierpiński Fractals. *ACS Photonics* **2019**, *6*, 2974–2984.

(35) Campos, A.; Arbouet, A.; Martin, J.; Gérard, D.; Proust, J.; Plain, J.; Kociak, M. Plasmonic Breathing and Edge Modes in Aluminum Nanotriangles. *ACS Photonics* **2017**, *4*, 1257–1263.

(36) Guzzinati, G.; Béché, A.; Lourenço-Martins, H.; Martin, J.; Kociak, M.; Verbeeck, J. Probing the Symmetry of the Potential of Localized Surface Plasmon Resonances with Phase-Shaped Electron Beams. *Nat. Commun.* **2017**, *8*, 1–8.

(37) Wen, F.; Zhang, Y.; Gottheim, S.; King, N. S.; Zhang, Y.; Nordlander, P.; Halas, N. J. Charge Transfer Plasmons: Optical Frequency Conductances and Tunable Infrared Resonances. *ACS Nano* **2015**, *9*, 6428–6435.

(38) Mortensen, N. A.; Raza, S.; Wubs, M.; Søndergaard, T.; Bozhevolnyi, S. I. A generalized non-local optical response theory for plasmonic nanostructures. *Nat. Commun.* **2014**, *5*, 3809.

(39) Aslan, E.; Aslan, E.; Wang, R.; Hong, M. K.; Erramilli, S.; Turkmen, M.; Saracoglu, O. G.; Dal Negro, L. Multispectral Cesaro-Type Fractal Plasmonic Nanoantennas. *ACS Photonics* **2016**, *3*, 2102–2111.

(40) Rodrigo, D.; Tittl, A.; John-Herpin, A.; Limaj, O.; Altug, H. Self-Similar Multiresonant Nanoantenna Arrays for Sensing from Near- to Mid-Infrared. *ACS Photonics* **2018**, *5*, 4903–4911.

(41) Gottheim, S.; Zhang, H.; Govorov, A. O.; Halas, N. J. Fractal Nanoparticle Plasmonics: The Cayley Tree. *ACS Nano* **2015**, *9*, 3284–3292.

(42) Alexander, C.; Giblin, I.; Newton, D. Symmetry groups of fractals. *The Mathematical Intelligencer* **1992**, *14*, 32–38.

(43) Harris, N.; Arnold, M. D.; Blaber, M. G.; Ford, M. J. Plasmonic Resonances of Closely Coupled Gold Nanosphere Chains. *J. Phys. Chem. C* **2009**, *113*, 2784–2791.

(44) Li, K.; Stockman, M. I.; Bergman, D. J. Self-Similar Chain of Metal Nanospheres as an Efficient Nanolens. *Phys. Rev. Lett.* **2003**, *91*, 227402.

(45) Wallace, G. Q.; Lagugné-Labarthet, F. Advancements in fractal plasmonics: structures, optical properties, and applications. *Analyst* **2018**, *144*, 13–30.

(46) Palik, E. D., Ed. *Handbook of Optical Constants of Solids*; Academic Press: Burlington, Ontario, 1997.

(47) Luke, K.; Okawachi, Y.; Lamont, M. R. E.; Gaeta, A. L.; Lipson, M. Broadband Mid-Infrared Frequency Comb Generation in a Si_3N_4 Microresonator. *Opt. Lett.* **2015**, *40*, 4823–4826.

(48) Hohenester, U. Simulating Electron Energy Loss Spectroscopy with the MNPBEM Toolbox. *Comput. Phys. Commun.* **2014**, *185*, 1177–1187.

(49) Johnson, P. B.; Christy, R. W. Optical Constants of the Noble Metals. *Phys. Rev. B* **1972**, *6*, 4370–4379.

(50) Fredkin, D. R.; Mayergoyz, I. D. Resonant Behavior of Dielectric Objects (Electrostatic Resonances). *Phys. Rev. Lett.* **2003**, *91*, 253902.

(51) Bicket, I. C. SpectrumImageAnalysisPy: 3D Spectrum Image analysis for electron energy loss spectroscopy and cathodoluminescence. 2019; `https://github.com/icbicket/SpectrumImageAnalysisPy`, original date: 2016-09-10. DOI: 10.5281/zenodo.807762.

(52) Bellido, E. P.; Rossouw, D.; Botton, G. A. Toward 10 meV Electron Energy-Loss Spectroscopy Resolution for Plasmonics. *Micros. Microanal.* **2014**, *20*, 767–778.

Graphical TOC Entry